Regional Studies in Marine Science 44 (2021) 101796

Contents lists available at ScienceDirect

Regional Studies in Marine Science

journal homepage: www.elsevier.com/locate/rsma

# Sea surface $pCO_2$ variability and air-sea $CO_2$ exchange in the coastal Sudanese Red Sea

Elsheikh B. Ali [a], Ingunn Skjelvan [b,*], Abdirahman M. Omar [b], Are Olsen [c], Tor E. de Lange [c], Truls Johannessen [c], Salma Elageed [c,a]

[a] Institute of Marine Research, Red Sea University, Port Sudan, Sudan
[b] NORCE Norwegian Research Centre, Bjerknes Centre for Climate Research, Bergen, Norway
[c] Geophysical Institute, University of Bergen and Bjerknes Centre for Climate Research, Bergen, Norway

ARTICLE INFO

*Article history:*
Received 9 November 2020
Received in revised form 16 April 2021
Accepted 17 April 2021
Available online 20 April 2021

*Keywords:*
Sea surface $pCO_2$
$CO_2$ flux
Time series
Coastal Red Sea
Seasonality

ABSTRACT

The dynamics of sea surface $pCO_2$ ($pCO_2^w$) and air–sea $CO_2$ exchange of the Sudanese coastal Red Sea has for the first time been studied over a full annual cycle (October 2014–October 2015) based on semi-continuous measurements from moored autonomous sensors. $pCO_2^w$ showed a seasonal amplitude of approximately 70 μatm, overlaid by a high frequency (3-4 days) signal of around 10 μatm. The highest values, of about 440 μatm occurred during summer and fall, while the lowest values of about 370 μatm occurred during winter. The monthly $pCO_2^w$ change was primarily driven by temperature, i.e., heating and cooling of the water surface. Additionally, Dissolved Inorganic Carbon (DIC) and Total Alkalinity (AT) contributed significantly to the observed change in $pCO_2^w$ as a consequence of along-coast advection and upwelling of $CO_2$-rich deep water, and likely biological production, and uptake of atmospheric $CO_2$. The area is a net annual source for atmospheric $CO_2$ of 0.180 ± 0.009 mol $CO_2$ $m^{-2}$ $y^{-1}$. Based on a compilation of historic and our new data, altogether covering the years 1977 to 2015, long term trends of $pCO_2^w$ were determined for the seasons winter–spring (1.75 ± 0.72 μatm $y^{-1}$) and summer -fall (180 ± 0.41 μatm $y^{-1}$), both weaker than the atmospheric trend (1.96 ± 0.02 μatm $y^{-1}$). We are suggesting that the study region has transformed from being a source of $CO_2$ to the atmosphere throughout the year to becoming a sink of $CO_2$ during parts of the year. The long term $pCO_2^w$ trend was to a large degree driven by increasing DIC, but increasing AT and temperature also played a role.



## 1. Introduction

Anthropogenic emissions of carbon dioxide ($CO_2$) into the atmosphere result from burning of fossil fuel and land use change. During the last decade (2009–2018) these processes have been responsible for an input to the atmosphere of 9.5 ± 0.5 Pg C $y^{-1}$ (Friedlingstein et al., 2019), of which the ocean and terrestrial biosphere have absorbed about 2.5 ± 0.6 and 3.2 ± 0.6 Pg C $y^{-1}$, respectively (Friedlingstein et al., 2019). The global carbon budget is based on an enormous amount of data from all over the world, but there is still an ongoing effort to more precisely determine the amount of carbon exchanged between the different reservoirs. Generally, an improved understanding of the ocean $CO_2$ variability is needed since models seem to underestimate this (Friedlingstein et al., 2019). On a regional scale, the marginal seas are generally not considered in the global carbon budget presented by Friedlingstein et al. (2019), and this is also the case for climatology like Takahashi et al. (2002). The current knowledge of the carbon cycle in these regions is still insufficient to derive precise information for climate change prediction (Dai et al., 2013; Laruelle et al., 2017; Ali, 2008), and it is still not clear why some coastal regions act as a source for $CO_2$ while others seem to be sources for $CO_2$ (Dai et al., 2013).

The Red Sea is a narrow sea connecting the Mediterranean Sea and the Indian Ocean. It is one of the warmest and saltiest seas in the world, with surface water temperatures of 26–30°C and salinities of 36–41. Recently, Chaidez et al. (2017) showed that the Red Sea is warming at a rate of 0.17 ±0.07 °C $decade^{-1}$, which is higher than the global trend of 0.11 °C $decade^{-1}$ Rhein et al., 2013. The evaporation from the Red Sea is extremely high (1.6–1.9 m $y^{-1}$; Tragou et al., 1999), the precipitation is in the other end of the scale (0.05 m $y^{-1}$; Zolina et al., 2017), and the sea receives negligible freshwater input from land (Sofianos and Johns, 2002). The low precipitation and lack of river runoff limit the erosion in the area (Rasul et al., 2015), which might be one of several reasons for the observed reduction in calcification rates in the Red Sea (Steiner et al., 2018). The Red Sea has an

* Corresponding author.
*E-mail address:* insk@norceresearch.no (I. Skjelvan).

https://doi.org/10.1016/j.rsma.2021.101796

exceptionally rich biodiversity which is supported by coral reefs that extends thousands of kilometres along the coast (Klaus, 2015, and references therein). Although the productivity is low, the sea supports fisheries (mainly artisanal) that are an important source of proteins in the region (FAO, 1989). The Red Sea is also known for its recreational diving sites and a dozen popular tourist destinations.

The Red Sea is heavily under sampled and for this reason, only limited knowledge regarding the inorganic carbon cycle and air–sea $CO_2$ exchange is available in the literature. This is particularly true for the western coastal areas (Rasul et al., 2015). Surveys have typically been conducted along the north–south central axis of the Red Sea, such as: the GEOSECS cruise in 1977 (Weiss et al., 1983), the MEROU cruises in 1982 (Beauverger, 1984a; Beauverger et al., 1984b; Souvermezoglou et al., 1989; Metzl et al., 1989), and the MINERVE cruises in 1991, 1992, and 1999 (Metzl et al., 1995; Metzl, 2016). Consistently, these have shown that the Red Sea is a source of $CO_2$ to the atmosphere, which was later confirmed by Ali (2008), who used the above-mentioned data in addition to western coastal Red Sea data from 2007. Souvermezoglou et al. (1989) used two methods (direct and indirect) to determine a carbon budget for the summer and the winter in the Strait of Bab-El-Mandab at the entrance of the Red Sea. They concluded that the Red Sea is a source for $CO_2$ during both seasons. Metzl et al. (1989) used GEOSECS (December 1977; Weiss et al., 1983) and MEROU (June and October 1982; Beauverger, 1984a; Beauverger et al., 1984b) data to initialize an inverse model for transport and carbon exchange. In their model, the air–sea $CO_2$ flux evaded into the air during both summer and winter. In Metzl et al. (1995), data from the MINERVE cruises, which primarily covered the Indian Ocean, were presented, and the Red Sea appeared to be a source for $CO_2$ to the atmosphere, as previous studies had shown. Metzl et al. (1995) showed, however, that the size of the $CO_2$ source decreased from south to north, and the northernmost part of this enclosed sea was a sink during the summer of 1991.

The surveys GEOSECS (Weiss et al., 1983), MEROU (Beauverger, 1984a; Beauverger et al., 1984b; Souvermezoglou et al., 1989; Metzl et al., 1989), MINERVE (Metzl et al., 1995; Metzl, 2016), and that of the coastal western Red Sea (Ali, 2008) were conducted during limited periods of time (i.e. December, June, October). Reconstructed $pCO_2$ fields (e.g., Denvil-Sommer et al., 2019; CMEMS, 2019; Landschützer et al., 2020) exist over the full annual cycles, however, there is a lack in $pCO_2$ observations collected over longer amount of time in the Red Sea, and thus, it is difficult to estimate annual estimates of the $CO_2$ flux in the area with high degree of confidence.

In this study, we investigate the seasonal dynamics of sea surface partial pressure of $CO_2$ ($pCO_2^w$) and air–sea $CO_2$ exchange in the Sudanese coastal Red Sea off Port Sudan (Fig. 1) using new carbon and hydrography data. We present, for the first time in this area, the full annual cycle of $pCO_2^w$ and determine the drivers of the seasonal $pCO_2^w$ variations. Further, we determine the long-term trend of the $pCO_2^w$ in the central Red Sea and discuss the associated drivers.

## 2. Data and methods

### 2.1. Data

The data used in this study are collected from one mooring equipped with two instruments deployed in Sudanese coastal waters over the period 2014–2015. In addition, we used data from the open sea collected through international expedition (GEOSECS, Weiss et al., 1983; MEROU, Beauverger, 1984a; Beauverger et al., 1984b; Souvermezoglou et al., 1989; Metzl et al., 1989; MINERVE, Metzl et al., 1995; Metzl, 2016; VOS_Pacific_Celebes, Hydes et al., 2011) and data from a coastal carbon time series (2007 and 2009–2013, (Ali, 2017), see Fig. 1 and Table 1.

The moored instruments were deployed in October 2014 and retrieved one year later, in October 2015. The mooring, positioned at 37.395 ° E, 19.720 ° N, was located 18 km north east of Port Sudan at the Sudanese coast (Fig. 1), at the same position as one of the stations in the coastal carbon time series (Ali, 2017). The moored instruments were a Sea Bird MicroCat (SBE 37-SM) with temperature and conductivity sensors (accuracy ±0.01 °C and ± 0.02 mS $cm^{-1}$, respectively) and a SAMI-$CO_2$ (Submersible Autonomous Moored Instrument) sensor from Sunburst Sensors ($pCO_2$ accuracy ± 3 μatm based on factory calibration to NIST traceable infrared detector). The bottom depth at the mooring site is about 800 m, and the MicroCat and SAMI-$CO_2$ were positioned at 37 and 34 m depth, respectively. Temperature and conductivity were determined hourly, while the $pCO_2^w$ was measured every three hours throughout the year of deployment. To evaluate the SAMI sensor $pCO_2^w$ measurements, discrete samples of DIC (Dissolved Inorganic Carbon) and AT (Total Alkalinity) were collected from 40 m depth immediately after the mooring deployment and at the time of mooring retrieval a year later. Unfortunately, the samples collected during retrieval were destroyed during transport. The DIC and AT samples were conserved using saturated $HgCl_2$ solution, kept cold and dark, and analysed at the Geophysical Institute, University of Bergen, Norway, 7 weeks after collection. DIC was determined using gas extraction of acidified water samples followed by coulometric titration (Johnson et al., 1993; Dickson et al., 2007) with a VINDTA 3C interfaced with a UIC Coulometer (CM5012, accuracy ± 2 μmol $kg^{-1}$), while AT was analysed using an open cell titration system; the Marianda VINDTA 3S (accuracy ± 2 μmol $kg^{-1}$). The accuracy was determined by using certified reference material (CRM) supplied by prof. Andrew Dickson, Scripps Institution of Oceanography, USA. Further, the software CO2SYS (van Heuven et al., 2011) with the carbon system constants of Mehrbach et al. (1973) refitted by Dickson and Millero (1987), $KSO_4^-$ constant from Dickson (1990), and total boron from Uppström (1974) was used to calculate $pCO_2^w$. Comparison between the SAMI $pCO_2^w$ measurements and the calculated $pCO_2^w$ resulted in an adjustment of the SAMI $pCO_2^w$ measurements of +15.7 μatm. In addition, the mooring $pCO_2^w$ data were compared with calculated $pCO_2^w$ from a coastal carbon time series described in Ali (2017), where monthly averaged DIC and AT over 4–40 m depth and constants as above were used as input to CO2SYS (van Heuven et al., 2011). Average offset between the mooring $pCO_2^w$ and the time series $pCO_2^w$was 5.3 μatm with a standard error of 4.8 μatm (n=7).

Atmospheric $xCO_2$ ($pCO_2^{air}$) measurements from the nearest station (Sede Boker in Negev desert, Israel) were downloaded from NOAA/CMDL (http://cdiac.ornl.gov/trends/co2/cmdl-flask/wis.html) (Dlugokencky and Tans, 2020), and atmospheric $pCO_2$ ($pCO_2^{air}$) values were calculated according to Körtzinger (1999) using standard atmospheric air pressure (1013.25 mbar).

The coastal carbon time series are described in (Ali, 2017), and only a brief description is included here. The time series consist of DIC, AT, temperature and salinity, which were collected between Port Sudan and Sanganeb atoll reef located 30 km northeast of Port Sudan (Fig. 1 and Table 1). Samples for the coastal time series were collected at 4 m depth from 10 stations in July 2007 (SPS1 section; (Ali, 2017), while over the years 2009–2013, samples were collected from 4 m depth from 5 stations (St1, St2, St3, St5, St6) and from 4–60 m depth from one station (St4) (SPS2 section; (Ali, 2017). The SP2 section was sampled 2–4 times each year, typically February, April, July, and October.

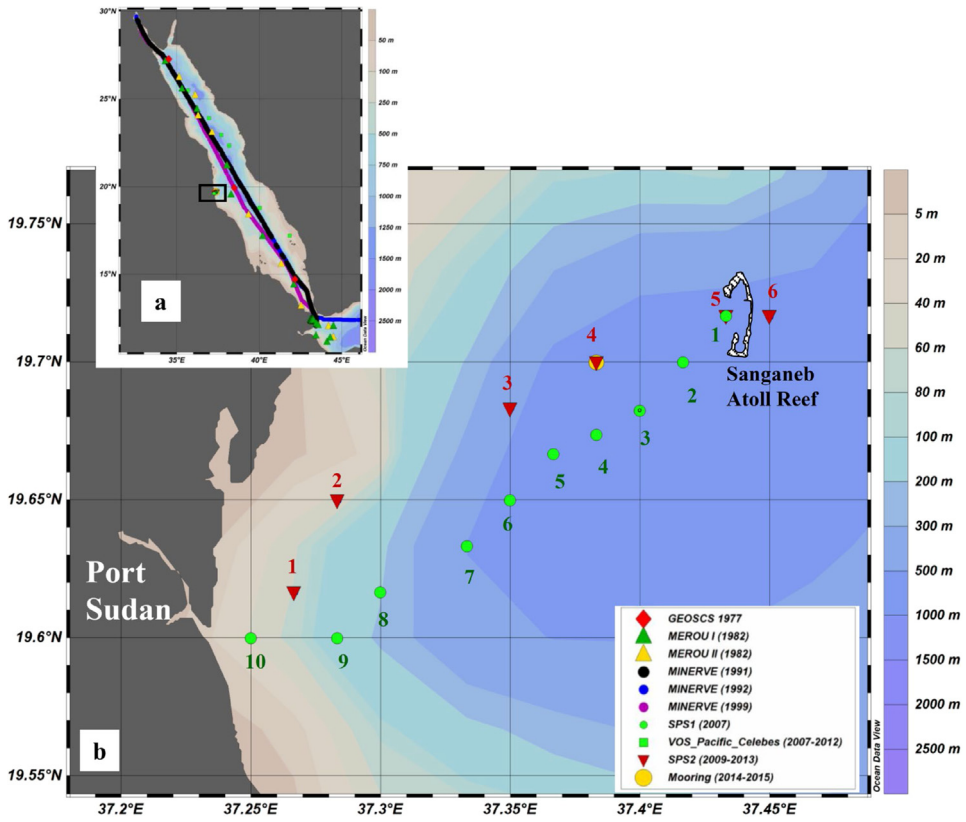


**Fig. 1.** (a) The Red Sea with locations of the different datasets used in this study (plot made in Ocean Data View; Schlitzer, 2020). The coastal study area is enclosed in the black-bordered box at the Sudanese coast. (b) The location of the mooring between Port Sudan and Sanganeb atoll reef is indicated (yellow circle), together with the coastal carbon time series (SPS1 and SPS2), green circles and red triangles) described in Ali (2017) and Ali et al. (2018). Note that the mooring position is the same as that of station 4 (St4) in the coastal carbon time series SPS2.

### 2.2. Data processing

Ali et al. (2018) examined in detail the seasonal variations of the water masses along the section between Port Sudan and the Sanganeb atoll reef (Fig. 1). They found that the mixed layer depth (MLD) is approximately 40 m deep during most of the year and deeper during winter mixing, and thus, the water shallower than 40 m is part of a homogeneous surface layer. To examine if this was also the case for $pCO_2^w$, the coastal carbon time series in Ali (2017) was used to calculate monthly averaged $pCO_2^w$ (software and constants as described in Section 2.1) at two depth levels: 4 m and 30–40 m. The difference between calculated $pCO_2^w$ at 4 m and 30–40 m was on average 8.6 μatm, which was half the average variability within the calculated $pCO_2^w$ at 4 m depth (19 μatm). Thus, it is reasonable to assume that the mooring data from 34 and 37 m depth in the current study represents the surface. On a few occasions, the moored instruments were pulled down to 42–48 m, apparent from the Sea-Bird MicroCat pressure data (not shown). This happened e.g., towards the end of July and September 2015; however, no noticeable changes were observed in $pCO_2^w$, salinity or temperature during these events, and consequently, these data are included in the analyses.

The net air–sea $CO_2$ flux ($F_{CO2}$) was determined using the $pCO_2$ difference between the seawater ($w$) and atmosphere ($air$):

$$F_{Co_2} = KS\left(pCO_2^w - pCO_2^{air}\right) = KS\Delta pCO_2 \quad (1)$$

where $K$ is the gas transfer velocity and $S$ is the $CO_2$ solubility in seawater. $K$ is commonly parameterized as a function of wind-speed ten metres above the sea surface ($U_{10}$), and several studies have examined the relationship between $U_{10}$ and $K$ (e.g., Liss and Merlivat, 1986; Wanninkhof, 1992; Nightingale et al., 2000; Sweeney et al., 2007; Wanninkhof, 2014). At low wind speeds, the selection of $K$-$U_{10}$ relationship does not have a big impact on the calculated fluxes (e.g. Sweeney et al., 2007), but at wind speeds above approximately 5 m $s^{-1}$, the deviation between the various $K$-$U_{10}$ relationships becomes notable. In the current study, where wind speeds typically were less than 10 m $s^{-1}$ (Fig. 2e), the $K$-$U_{10}$ relationship from Nightingale et al. (2000) was used. This results in $K$ values that are similar to those determined using the relationship by Sweeney et al. (2007) for wind speeds below 10 m $s^{-1}$. $U_{10}$, was calculated from daily averaged 6-hourly u- and v-wind velocity components extracted from NCEP/NCAR reanalysis 2 data (https://climatedataguide.ucar.edu/climate-data/ncep-reanalysis-r2) at the position 20.00 °N and 37.50 ° E (Kalnay et al., 1996). The $CO_2$ solubility, $S$, was determined according to Weiss (1974).

The factors controlling monthly $pCO_2^w$ changes were quantified according to the framework of Takahashi et al. (1993), where temperature (SST), salinity (SSS), DIC, and AT contribute to the $pCO_2^w$ change:

$$\Delta pCO_2 = \frac{\partial pCO_2}{\partial SST}\Delta SST + \frac{\partial pCO_2}{\partial SSS}\Delta SSS + \frac{\partial pCO_2}{\partial DIC}\Delta DIC + \frac{\partial pCO_2}{\partial AT}\Delta AT \quad (2)$$

This equation is rearranged to the following form:

$$\Delta pCO_2 = \tau pCO_2\Delta SST + \eta pCO_2\Delta SSS + \gamma pCO_2\Delta DIC + \Gamma pCO_2\Delta AT \quad (3)$$

where $\tau$ = 0.0423 °$C^{-1}$, $\eta$ = 0.9, $\gamma$ = 8.6, and $\Gamma$ = -7.0. The two first ($\tau$ and $\eta$) were determined from Takahashi et al. (1993), while the two latter ($\gamma$ and $\Gamma$), which are the Revelle factors for

**Table 1**
Data sources in the central Red Sea (19 - 20°N, 36.2 – 39.6°E) used to determine surface trends of $pCO_2^w$ and their drivers.

| Name/year | Dataset characteristics | Month of data | Stations used/ depth[a] | Variables[b] | Method for calculation | References |
|---|---|---|---|---|---|---|
| GEOSECS[c]/1977 | Discrete/water column/ open sea | Dec. | 1/6 – 30 m | T, S, P, AT, DIC, $O_2$, $PO_4$, $NO_2$, $NO_3$, $SiO_3$ | $pCO_2$ calc. from CO2SYS | Weiss et al. (1983) |
| MEROU I/1982 | Discrete/water column/ open sea | Jun. | 1/0 – 25 m | T, S, P, AT, DIC, $O_2$, PO4, $NO_2$, $NO_3$, $SiO_3$ | $pCO_2$ calc. from CO2SYS | Beauverger (1984a), Beauverger et al. (1984b), Souvermezoglou et al. (1989), Metzl et al. (1989) |
| MINERVE/1991 | Continuous/surface/ open sea | Jun. | 27/5 – 6 m | T, S, $pCO_2^w$ | AT from SSS, DIC calc. from CO2SYS | Metzl et al. (1995), Metzl (2016) |
| MINERVE/1992 | Continuous/surface/ open sea | Jun. | 27/5 – 6 m | T, S, $pCO_2^w$ | AT from SSS, DIC calc. from CO2SYS | Metzl et al. (1995), Metzl (2016) |
| MINERVE/1999 | Continuous/surface/ open sea | Oct. | 27/5 – 6 m | T, S, $pCO_2^w$ | AT from SSS, DIC calc. from CO2SYS | Metzl (2016) |
| VOS_Pacific_Celebes /2009 | Discrete/surface/ open sea | Apr. | 1/ 5 m | T, S, P, AT, DIC, $O_2$ | $pCO_2$ calc. from CO2SYS | Hydes et al. (2011) |
| Coastal carbon time series (SPS1)/2007 | Discrete/surface/ coastal | Jul. | 10/ 4 m | T, S, AT, DIC | $pCO_2$ calc. from CO2SYS | Ali (2017) |
| Coastal carbon time series (SPS2)/2009 | Discrete/water column/ coastal | Oct., Dec. | 6/ 4 m | T, S, P, AT, DIC | $pCO_2$ calc. from CO2SYS | Ali (2017) |
| Coastal carbon time series (SPS2)/2010 | Discrete/water column/ coastal | Feb., Apr., Jul., Oct. | 6/ 4 m | T, S, P, AT, DIC | $pCO_2$ calc. from CO2SYS | Ali (2017) |
| Coastal carbon time series (SPS2)/2011 | Discrete/water column/ coastal | Feb., Apr., Jul., Oct. | 6/ 4 m | T, S, P, AT, DIC | $pCO_2$ calc. from CO2SYS | Ali (2017) |
| Coastal carbon time series (SPS2)/2012 | Discrete/water column/ coastal | Feb., Jul., Oct. | 6/ 4 m | T, S, P, AT, DIC | $pCO_2$ calc. from CO2SYS | Ali (2017) |
| Coastal carbon time series (SPS2)/2013 | Discrete/water column/ coastal | Feb., Apr., Jul., Oct. | 6/ 4 m | T, S, P, AT, DIC | $pCO_2$ calc. from CO2SYS | Ali (2017) |
| Mooring data/ 2014–2015 | Semi-continuous/surface/ coastal | Oct.-Sep. | 365/ 37 m | T, S, P, $pCO_2^w$ | AT from SSS, DIC calc. from CO2SYS | This study |

[a]The number of stations used to calculate monthly means.
[b]T= temperature S=salinity; P=pressure (depth).
[c]The data were adjusted by Olsen et al. (2016) and Key et al. (2015).

DIC and AT, respectively, were determined by using the averaged values from 0–40 m deep of the coastal carbon time series (Ali, 2017) as input in the CO2SYS software (van Heuven et al., 2011).

Further, to examine the factors controlling $pCO_2^w$ changes, AT and DIC data over a full year are required, according to Eq. (3). Daily AT data were reconstructed from mooring salinity, using the linear regression: AT = 35.3 S + 1070 ($R^2$ = 0.44), which was developed from the coastal carbon time series described in Ali (2017) and Ali et al. (2018) selecting data from 2009–2013 and 4 to 40 m depth (Fig. S.1 in Supplementary material). Our AT-SST relationship was similar to that of Steiner et al. (2018); their Fig. 3; y=35.78 S +1076, $R^2$=0.91) and that of surface (0–50 m) MEROU data from three stations closest to the mooring site in the current study (y=34.89 S +1078, $R^2$=0.86; Fig. S.1 in Supplementary material). The $R^2$ of 0.44 in our AT-SSS relationship indicate that S can explain only about 40% of the AT variation in the coastal area. Thus, by using our AT-SSS relationship for TA computation possible changes in AT from other processes are neglected. This highlights the need for better understanding of the observed AT variations, however, an in-depth analysis of this is out of scope for this paper. Further, daily DIC was calculated from the reconstructed AT, mooring $pCO_2^w$ salinity, and temperature using CO2SYS (van Heuven et al., 2011). Nutrient concentrations were assumed to be zero in these calculations, which induced an error in calculated $pCO_2^w$ of less than 2 μatm. The drivers for the observed $pCO_2^w$ changes were determined on a monthly basis, where the change in monthly $pCO_2^w$ represents the difference from one month to the subsequent month.

## 3. Results

The summer season is defined as the months May–August while the winter is December–February, as in Ali et al. (2018). Spring and fall months are March–April and September–November, respectively. For the coastal Red Sea, the seasonal cycle is the primary mode of variability (Fig. 2a–c), but there is also higher frequency (3–4 days) variability (Fig. 2c). The seasonal temperature change was about 6 °C (Fig. 2a) while that of salinity was approximately 1.1 (Fig. 2b). The highest temperatures occurred during fall and the lowest at the end of January, while the summer was a transition period with relatively large variations over short times. In mid-May, the temperature abruptly increased to its average summer value of 28.5 °C. The salinity (Fig. 2b) was highest (approximately 40) during fall and winter and lowest (around 38.7) during spring and summer. Several abrupt and large changes in salinity occurred, e.g., in early March and in late August (Fig. 2b). The seasonal peaks and lows for the salinity lagged those of temperature by about 3 months, which, according to Ali et al. (2018) most likely is caused by temperature variation being governed by air–sea heat exchange in addition to horizontal fluxes associated with advection of water along the coast. This transports fresher water from the south into the area of study (Ali et al., 2018), which partly explains the observed salinity variation,

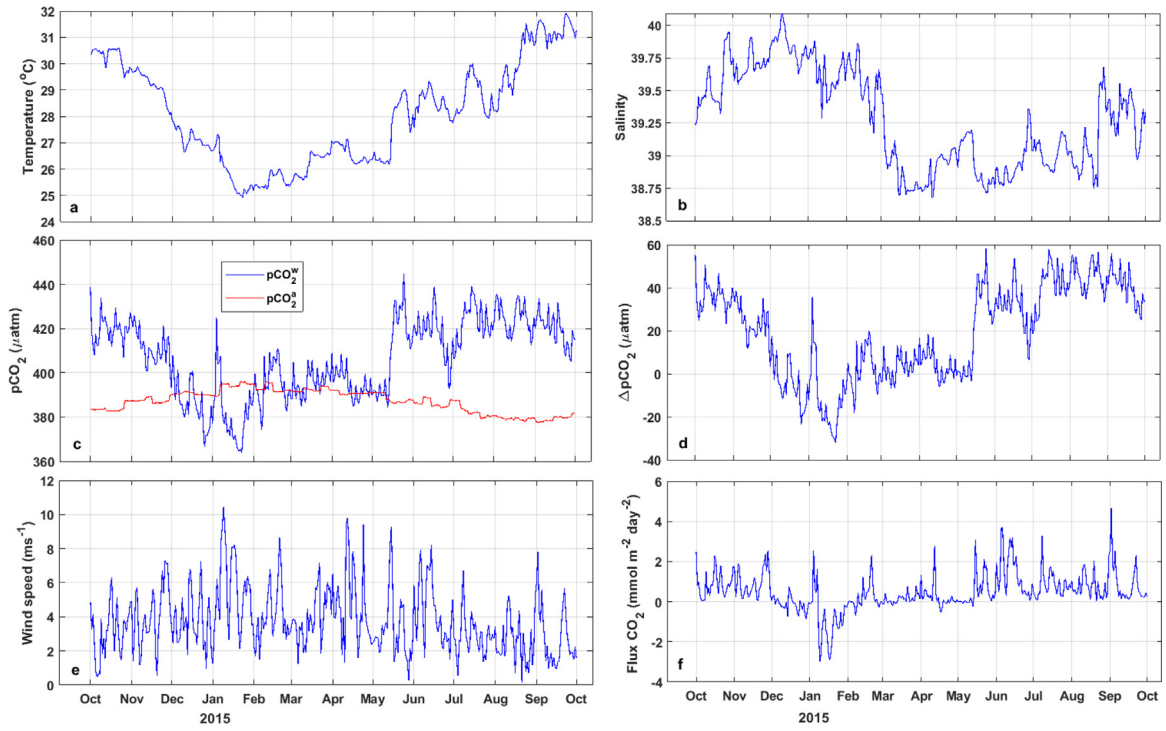


**Fig. 2.** Daily average of (a) temperature (°C), (b) salinity, (c) $pCO_2^{air}$ and $pCO_2^{w}$ (μatm), (d) $\Delta pCO_2$ (μatm), (e) wind speed (m $s^{-1}$), and (f) $CO_2$ fluxes (mmol $CO_2$ $m^{-2}$ $day^{-1}$). Positive $\Delta pCO_2$ and $F_{CO2}$ indicate gas transport from sea to air. The horizontal ticks represent day one in a month.

while evaporation and precipitation are additional factors, with evaporation dominating.

The $pCO_2^{w}$ followed the temperature during parts of the year (Fig. 2c), with a seasonal amplitude of approximately 70 μatm, and a higher frequency (3–4 days) signal of about 10 μatm. The correlation between daily $pCO_2^{w}$ and SST is relatively strong ($R^2$=0.6; Supplementary material, Fig. S2). The highest $pCO_2^{w}$ occurred during late summer and fall (approximately 440 μatm) when the water was warmest, while the lowest $pCO_2^{w}$ was observed in January (ca. 370 μatm) when the water was coldest. During spring, the $pCO_2^{w}$ value was relatively stable, which was also the case for temperature and to some degree salinity. Abrupt $pCO_2^{w}$ changes occurred during early January and mid-May, where the first was a sharp and short-lasting peak, most likely connected to wind speed, while the latter was a sharp transition to summer conditions when warmer and less saline surface water was advected from the south. This was also seen as a simultaneously abrupt decrease in salinity (0.5) and increase in temperature (about 2 °C; Fig. 2b).

The atmospheric $pCO_2$ ($pCO_2^{air}$, Fig. 2c) was highest during winter and spring and lowest during summer, with a seasonal amplitude of about 15 μatm, i.e., 25% of that of $pCO_2^{w}$. The seasonal cycle of $\Delta pCO_2$ (Fig. 2d, Eq. (1)), was thus governed by the $pCO_2^{w}$. The region was undersaturated with respect to $CO_2$ in parts of the winter while during the rest of the year, the ocean was supersaturated.

The daily $CO_2$ fluxes ($F_{CO2}$) are shown in Fig. 2f, and the values were periodically low, a result of low wind speeds and periods of near $CO_2$ equilibrium between ocean and atmosphere. Over the year, the flux was highly variable and mostly directed from ocean to atmosphere, with $CO_2$ being degassed to the atmosphere at a rate of up to 4.7 mmol $CO_2$ $m^{-2}$ $day^{-1}$. During winter 2015, a significant $CO_2$ undersaturation ($\Delta pCO_2$ up to −32 μatm) developed and in late January, the area was a sink for atmospheric $CO_2$ with fluxes as high as -3 mmol $CO_2$ $m^{-2}$ $day^{-1}$. The strongest $CO_2$ uptake occurred during events of high wind speeds (Fig. 2e), and over the year of 2014 to 2015, the area was a net source for atmospheric $CO_2$ of 0.180 ± 0.009 mol $CO_2$ $m^{-2}$ $y^{-1}$, where the uncertainty is the root sum of squares of the daily uncertainties over a year, and uncertainties of $U_{10}$ and $pCO_2^{w}$ were assumed to be ±1 m $s^{-1}$ and ±2 μatm, respectively.

## 4. Discussion

To quantify the drivers of the observed changes in $pCO_2^{w}$, a decomposition analysis as described in Eqs. (2) and (3) was performed, where the driving variables considered were sea surface temperature (SST), sea surface salinity (SSS), DIC, and AT. This is discussed in Section 4.1, while Section 4.2 focuses on the long-term trend in air–sea $CO_2$ exchange in the Red Sea over a period of nearly four decades from 1977 to 2015.

### 4.1. Factors controlling monthly change in oceanic $pCO_2$

DIC calculated from mooring $pCO_2^{w}$ and AT (from SSS) is presented in Fig. 3a while AT is plotted in Fig. 3b. Between September and February, DIC increased likely due to upwelling of colder waters with remineralized organic matter, however, during January also uptake of atmospheric $CO_2$ (Fig. 2f) contributed to the DIC increase. In February, DIC dropped strongly due to advection of fresher water from the south, described in Ali et al. (2018), and seen as decreasing salinity (Fig. 2b), which was also reflected in the AT in February (shown in Fig. 3b). The counteracting effect of SST and DIC was also seen during July and August, but this time with an opposite sign: warming of the water and decreasing DIC likely due to net primary production.

The decomposition analysis was performed by using monthly averages of the mooring data, with the aim to quantify the drivers of the seasonal changes. However, we are aware of that monthly averages will smoothen the abrupt changes in $pCO_2^{w}$ (Fig. 2c) as well as the high frequency $pCO_2^{w}$ variability that occurred on top of the seasonal cycle.

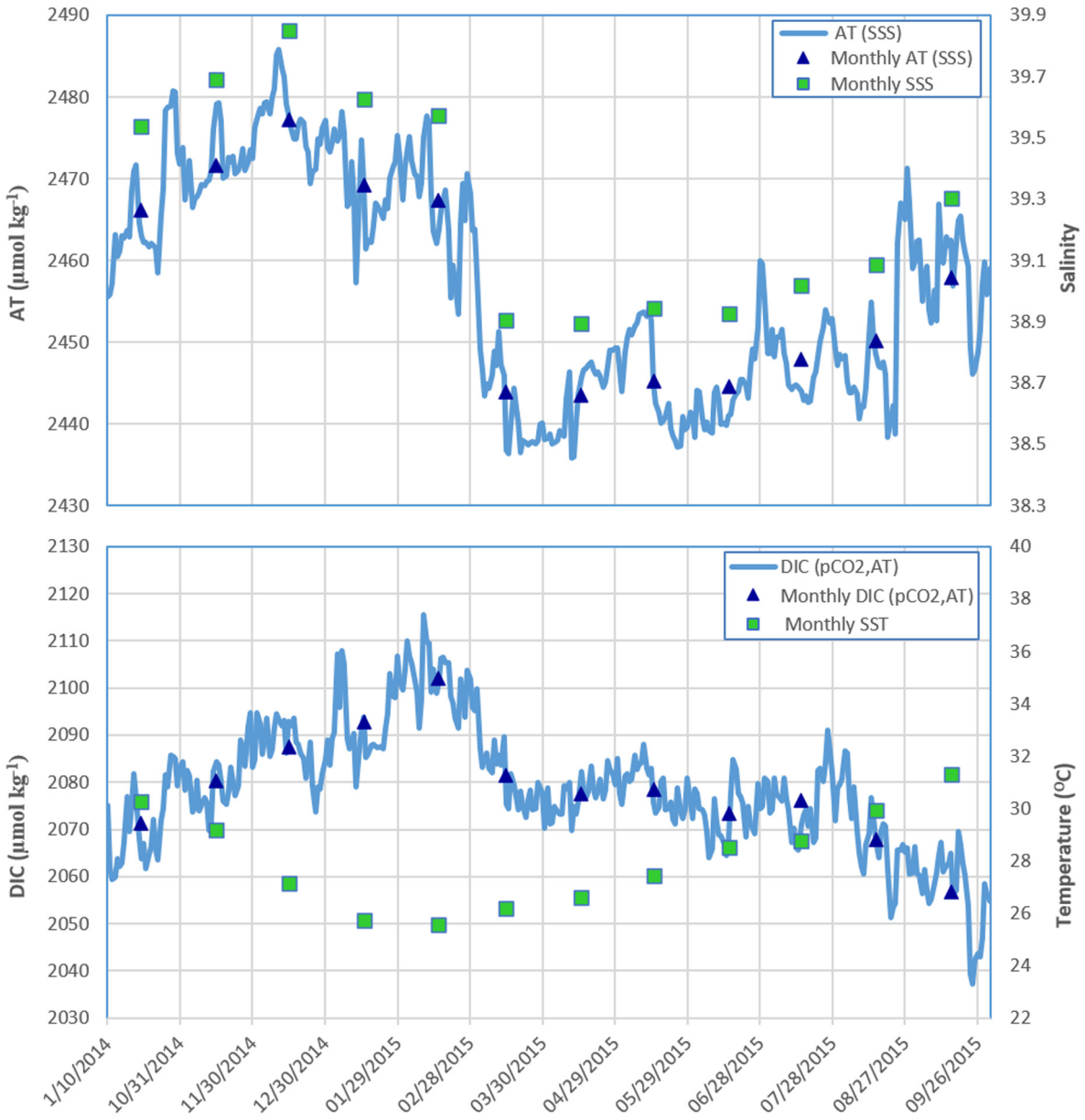


**Fig. 3.** Upper: The seasonal cycle of AT (estimated from SSS) (blue line) and the accompanying monthly average (blue triangles). Monthly SSS averaged from mooring data (green squares) and are also shown. Lower The seasonal cycle of DIC calculated from mooring $pCO_2^w$ and AT (estimated from SSS) (blue line) and the accompanying monthly average (blue triangles). Monthly SST averaged from mooring data (green squares) are also shown.

Fig. 4a shows the monthly changes in measured $pCO_2^w$ over a year, and the plot is similar to that of Fig. 4b, which represents the sum of the calculated drivers. Thus, it is reasonable to believe that the decomposition approach was representative for the situation in the coastal Red Sea.

Changes in temperature (Fig. 4c) was a strong driver for the $pCO_2^w$ changes, but DIC also contributed to the observed changes in $pCO_2^w$ (Fig. 4e). From September 2014 to January 2015, the surface water was cooling (Figs. 2a and 3a), which lowered the $pCO_2^w$ (Fig. 4c). From February to August, on the contrary, the SST increased (Figs. 2a and 3a), and induced a $pCO_2^w$ increase (Fig. 4c). Effects of SSS are overall negligible (Fig. 4d), except in February 2015 (representing the change from February to March), when freshening ($\Delta SSS = 1$) of the surface water led to a small negative change in $pCO_2^w$. This salinity change was described by Ali et al. (2018), who observed that during early February 2015, (their Fig. 4d) the geostrophic current in the area of study was reversed from southwards along-coast to northwards. This introduced water from the south with lower salinity combined with relatively higher temperature into the coastal area.

The strong drop in DIC (Fig. 3a) in February caused a highly negative change in $pCO_2^w$ (approximately -30 µatm; Fig. 4e), which was counteracted by a drop in AT caused by salinity change, corresponding to a positive change in $pCO_2^w$ of more than 20 µatm (Fig. 4f), and, thus, the net $pCO_2^w$ change was very low during this month. The increase in DIC between September and February (Fig. 3a) led to a corresponding positive change in $pCO_2^w$ (Fig. 4e), which to some degree counteracted the negative $pCO_2^w$ change induced by decreasing SST in January.

### 4.2. The long-term $pCO_2$ trend

The Red Sea is located in the sub-tropical area, which is globally characterized as a net annual source area of $CO_2$ (Takahashi et al., 2002). We have focused on the central Red Sea delimited by the box 19 - 20° N, 36.2 – 39.6 ° E (Fig. 5, upper

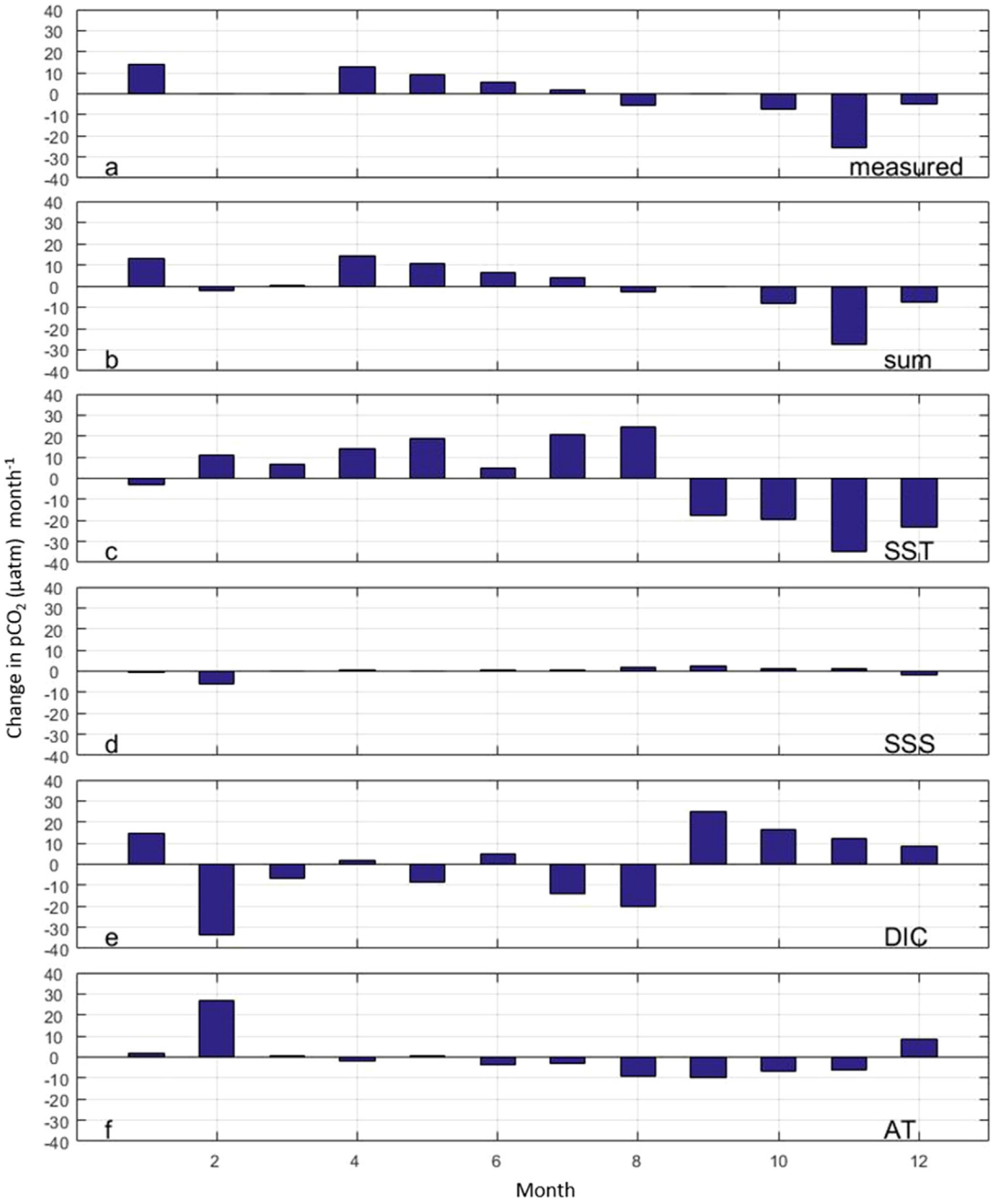


**Fig. 4.** Change in $pCO_2^w$ from one month to the next (µatm) (a) from measured data, (b) from sum of the drivers SST, SSS, DIC, and AT, (c) caused by SST, (d) caused by SSS, (e) caused by DIC, and (f) caused by AT. Note that the measured $pCO_2^w$ were collected from October 2014 to October 2015.

panel) and used data from GEOSECS 1977 (Weiss et al., 1983), MEROU I 1982 (Beauverger, 1984a; Beauverger et al., 1984b), MINERVE 1991, 1992, and 1999 (Metzl et al., 1995; Metzl, 2016), VOS_Pacific_Celebes 2009 (Hydes et al., 2011), coastal carbon time series (Ali, 2017), and the current study to estimate inter-annual trends of $pCO_2^w$ (Fig. 5). The trends cover the period 1977 to 2015 and are based on monthly means, however, some of the months only have one station (GEOSECS from December 1977, MEROU I from June 1982, and VOS_Pacific_Celebes from April 2009), while other months have more data points (e.g. MINERVE from June 1991, June 1992, and October 1999, and the coastal carbon time series from February 2010, 2011, 2012, and 2013).

The datasets with measured DIC, AT, SST and SSS, but no $pCO_2^w$ (GEOSECS, MEROU I, VOS_Pacific_Celebes, coastal carbon time series) were extended with calculated $pCO_2^w$ from CO2SYS (van Heuven et al., 2011) using DIC, AT, SST, and SSS as input. The dataset details are summarized in Table 1. DIC and AT data from the GEOSECS expedition were extracted from GLODAPv2 (Global Ocean Data Analysis Project) synthesis activity in which the data have been adjusted (Olsen et al., 2016; Key et al., 2015).

Motivated by the observation that the mooring area emitted $CO_2$ to the atmosphere during some seasons and absorbed atmospheric $CO_2$ during winter, the monthly means of $pCO_2^w$ from all cruises are split into winter–spring (GEOSECS, VOS_Pacific_Celebes, coastal carbon time series, and data from the current study) and summer-fall (MEROU I, MINERVE 1991, 1992, and 1999, coastal carbon time series, and data from the current study). The mean values and trends of $pCO_2^w$ are plotted in Fig. 5, and it should be bear in mind that both coastal and open ocean

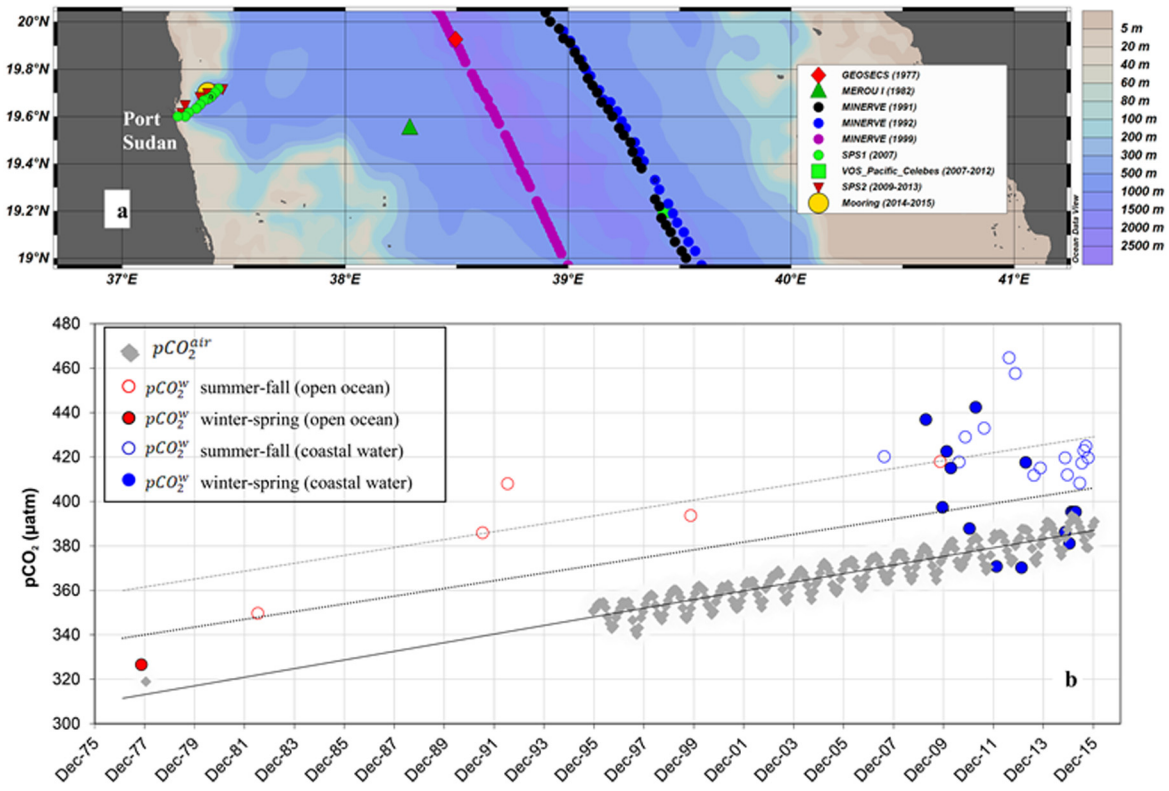


**Fig. 5.** Upper: A map showing locations of the data used in the trend plot below (Ocean Data View Schlitzer, 2020). Lower: Monthly averages and associated trend lines of $pCO_2^{air}$ from Sede Boker station (grey diamonds and grey line) and $pCO_2^{w}$ from GEOSECS 1977, MEROU I 1982, MINERVE 1991, 1992, and 1999, VOS_Pacific_Celebes 2009, coastal carbon time series (SPS1 and 2), and the current data. Summer–fall (May–November) $pCO_2^{w}$ data are indicated by open circles and dashed line, while winter–spring (December–April) $pCO_2^{w}$ data are the filled circles and dotted line. The red colour refers to open sea data, while blue colour refers to coastal data. The monthly averages are based on one station (GEOSECS, MEROU I, VOS_Pacific_Celebes) and multiple stations (MINERVE cruises, coastal carbon time series SPS1 and SPS2, and current mooring data). (For interpretation of the references to colour in this figure legend, the reader is referred to the web version of this article.)

data have been used to extend the number of years, which means that the results must be taken with care.

Fig. 5 also include monthly averages of $pCO_2^{air}$. These are based on atmospheric measurements from Sede Boker station in the Negev desert from 1995 and onwards. We have extrapolated the atmospheric data series back to 1977 by assuming a growth rate similar to that of Mauna Loa time series. This was checked by first comparing atmospheric $xCO_2^{air}$ values from Mauna Loa with those from the Sede Boker station. The seasonal amplitude was slightly larger at the latter station, but the interannual trend was similar at the two stations. Thus, it is reasonable to assume that the change in $xCO_2^{air}$ between 1977 and 1995 at the Israeli station was similar to the change in $xCO_2^{air}$ observed at Mauna Loa during the same period, i.e., 27 ppm. From this, we estimated the average $xCO_2^{air}$ value at Sede Boker to 338 ppm in 1977, which corresponds to a $pCO_2^{air}$ value of approximately 323 µatm (Fig. 5). Then, we could, with confidence, draw a line representing the monthly Red Sea $pCO_2^{air}$ over the years 1977–2015 (Fig. 5, grey line). The growth rate of $pCO_2^{air}$ over these nearly four decades is 1.96 ± 0.02 µatm $y^{-1}$ ($R^2$=0.9).

Fig. 5 shows that, over the years, the $pCO_2^{w}$ increase regardless of season. The trend of winter–spring $pCO_2^{w}$ (1.75 ± 0.72 µatm $y^{-1}$) is slightly weaker than that of summer-fall $pCO_2^{w}$ (1.80 ± 0.41 µatm $y^{-1}$) and both are weaker than the atmospheric $pCO_2^{air}$ trend. According to Souvermezoglou et al. (1989) and Metzl et al. (1989), the Red Sea was a year around source of $CO_2$ to the atmosphere. The data used in the current analysis are from both coastal and open ocean, however, we might speculate that, according to our findings of the area being a sink for $CO_2$ during winter, the year around $CO_2$ source must have changed at some point. It is difficult to determine when such a transformation might have occurred, but a similar transformation has previously been determined in the Mediterranean Sea. This sea was classified as a source of $CO_2$ during 1980s, while in the 2000s equilibria between $pCO_2^{w}$ and $pCO_2^{air}$ was reached, and at present the ocean is considered a minor sink of $CO_2$ (Taillandier et al., 2012). Their result was an average of the western and the eastern Mediterranean basin, where the western basin changed from being a weak sink of $CO_2$ during the 1980s to become a stronger sink in the 2000s, while the eastern basin changed from being a strong source to becoming a weaker source over the same period of time (Taillandier et al., 2012). The Red Sea is similar to the Mediterranean Sea in terms of being a semi-closed sea with relatively high temperature and salinity. Both seas are influenced by the same monsoon system, with north-northwesterly winds controlled by the Mediterranean weather system reaching all the way to Bab Al Mandab during summer. Thus, it is reasonable to assume that the same factors drive the source to sink transformation in the Mediterranean Sea and Red Sea. During summer-fall, when the $pCO_2^{w}$ trend (1.80 µatm $y^{-1}$) is less than the $pCO_2^{air}$ trend (1.96 µatm $y^{-1}$), the area emits a decreasing amount of $CO_2$ to the atmosphere from one year to the next. Thus, it is reasonable to assume that in the future, equilibrium might be reached between atmosphere and sea surface also during summer and fall. The coastal Red Sea might then be converted to a sink area for $CO_2$ throughout the year. These results have been compared with reconstructed monthly surface $pCO_2$ data from the Red Sea at 19.7 ° N 37.4 ° E. A neural network model (Denvil-Sommer et al., 2019) has been used for reconstruction, and the data were downloaded from Copernicus Marine Service (CMEMS, 2019). Over the years 1985 to 2019, the

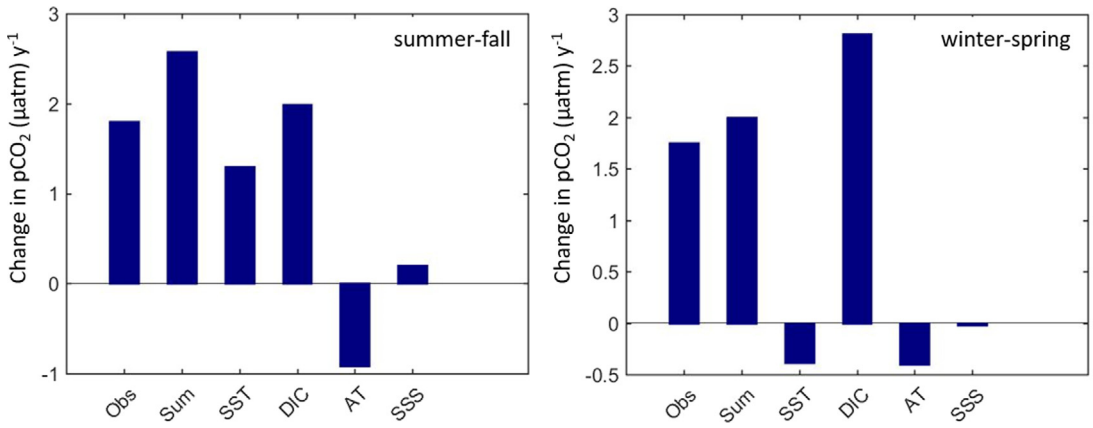


**Fig. 6.** Annual change in $pCO_2^w$ (µatm) from measured data (Obs), from sum of the drivers SST, DIC, AT, and SSS (Sum), caused by SST only (SST), caused by DIC only (DIC), caused by AT only (AT), and caused by SSS only (SSS). The plot to the left is from the summer–fall seasons, while that to the right is from the winter-spring seasons.

annual $pCO_2^w$ trend from reconstructed Red Sea data was +1.8 µatm $y^{-1}$ (Fig. S3 in Supplementary material). When focusing on the winter only (December–February), the $pCO_2^w$ trend was lower (1.5 µatm $y^{-1}$; Fig. S4 in Supplementary material). Thus, over the recent years this area of the Red Sea appeared to be a stronger $CO_2$ sink during winter compared to summer, which is in line with our results.

Over the longer period 1977 to 2015, the amount of surface $pCO_2^w$ data is low, and the assumption of the Red Sea was previously a year around $CO_2$ source must be drawn with care. The historical winter data are from the open ocean while the coastal data are not available until 2007. Therefore, it might be that the negative $CO_2$ fluxes are only apparent in the coastal area and not in the open ocean, which can only be unravelled by collecting more data.

Global warming leads to increasing SST, and this is described in Alawad et al. (2020) who found that for the period between 1982 and 2017 the annual mean SST in the northern half of the Red Sea has increased by about 0.04 °C $y^{-1}$. This is similar to the warming of the northern Red Sea of 0.4–0.45 °C $decade^{-1}$ found by Chaidez et al. (2017), but four times larger than the global warming trend of 0.11 °C $decade^{-1}$ (Rhein et al., 2013). If increasing temperature was the only factor influencing the $pCO_2^w$, the observed warming of the northern Red Sea would lead to a change in $pCO_2^w$ of about +20 µatm over the years 1977 to 2015. This would explain about a third of the observed $pCO_2^w$ trend of +1.71 µatm $yr^{-1}$. If, on the contrary, the warming rate of Chaidez et al. (2017) of +0.17 °C $decade^{-1}$ was used (average for the whole Red Sea and taking into consideration that the warming differs from region to region), this would increase the $pCO_2^w$ about 10 µatm over 38 years, i.e.about 15% of the observed $pCO_2^w$ trend. These estimates are, however, theoretical approaches, and it was shown in Fig. 4 that also DIC and to some degree AT contributed to the $pCO_2^w$ changes.

Further, higher SST will lower the solubility of $CO_2$, and thus slightly increase the $CO_2$ flux to the atmosphere (Weiss, 1974). This effect is counteracted by an increase in atmospheric $CO_2$ over time, which will decrease the $CO_2$ flux to the atmosphere in this area. Increasing SST will also result in more stratification of the upper ocean, which leads to less available nutrients from below and thus, reduced primary production (Behrenfeld et al., 2006; Raitsos et al., 2011; Taillandier et al., 2012). Low vertical mixing in $CO_2$ source areas like the Red Sea means less $CO_2$ exported from the deep layer into the surface, and consequently decreasing $CO_2$ levels in the surface layer. This, in turn, results in $CO_2$ equilibrium with the atmosphere and transformation into a sink area for atmospheric $CO_2$. Quantification of this has not been further elaborated due to lack of data.

**Table 2**
Long term trends in $pCO_2^w$ , DIC, SST, AT, and SSS over the years 1977–2015.

| Variables | Summer - fall Trends | 1 SD | Winter - spring Trends | 1 SD |
|---|---|---|---|---|
| $pCO_2^w$ (µatm $y^{-1}$) | 1.80 | 0.41 | 1.75 | 0.72 |
| DIC (µmol $kg^{-1}$ $y^{-1}$) | 1.14 | 0.36 | 1.71 | 0.24 |
| SST (°C $y^{-1}$) | 0.07 | 0.04 | −0.02 | 0.03 |
| AT (µmol $kg^{-1}$ $y^{-1}$) | 0.77 | 0.29 | 0.35 | 0.46 |
| SSS ($y^{-1}$) | 0.02 | 0.008 | −0.002 | 0.011 |

The long term trend in $pCO_2^w$ divided into the seasons summer-fall and winter–spring has been decomposed into drivers (SST, DIC, AT, SSS) similarly to the method described in Eqs. (2) and (3). Here, we have used the monthly means of $pCO_2^w$ developed for the trend analyses, and further, determined monthly means of SST, SSS, DIC, and AT for all datasets. The datasets, where only $pCO_2^w$, SSS and SST were measured (MINERVE 1991, 1992, 1999, and the current study) were extended with calculated TA from SSS using a AT-SSS relationship (see Section 2.2) based on data described in Ali (2017), and, further, DIC was calculated from CO2SYS(van Heuven et al., 2011) with AT, $pCO_2^w$, SST, and SSS as input as explained in Section 2. The results are presented in Fig. 6, and the SSS seems to be of negligible importance for the $pCO_2^w$ change over the years during the winter–spring seasons, while its importance increases slightly during the summer-fall seasons. DIC turns out to be the most important driver regardless of seasons. During the winter–spring seasons, DIC completely dominates over SST and TA, while during the summer-fall seasons, changes in SST and AT also play a role as drivers for the long term $pCO_2^w$ trend. The small and negative trend in SST during winter-fall (Table 2) is in contradiction to the observed warming of the area (Alawad et al., 2020; Chaidez et al., 2017), however, this trend value has a relatively high error (Table 2) and is not significant, likely due to few data before 2009. All year around, but strongest during summer-fall seasons, a positive change in AT induces a negative $pCO_2^w$ change. This is likely connected to the increasing AT observed along the central Red Sea between 1998 and 2018 by Steiner et al. (2018, their Fig. 2), which the authors connected to declining calcification rates in the central and southern Red Sea. An increase in AT over years (2007–2013; Ali, 2017) is also seen in the coastal carbon time series (not shown).

Table 2 presents the trend values for SST, DIC, AT, and SSS over the years in addition to their uncertainties (1 SD). The

uncertainties in Table 2 also reflect the uncertainties in Fig. 6 and is clear from their size that there are no significant trends in SST, SSS, and AT during winter–spring seasons, and thus, SST, SSS, and AT do not have significant effect as drivers during these seasons. The high uncertainties presented in Table 2 also contribute to the differences between the observed (Obs) trend in $pCO_2^w$ (change from one year to next) and the sum (Sum) of drivers.

## 5. Summary

We used data from a SAMI-$CO_2$ sensor moored at about 37 m depth in the coastal Red Sea off Port Sudan to study the annual cycle of oceanic $pCO_2$ ($pCO_2^w$) in the period October 2014–October 2015. The $pCO_2^w$ varied with a seasonal amplitude of approximately 70 $\mu$atm with highest values during summer and fall. The $pCO_2^w$ seasonality was overlaid with a high frequency (3–4 days) fluctuation of about 10 $\mu$atm. Decomposition analyses revealed that the seasonal changes in $pCO_2^w$ were mainly driven by changes in temperature, although DIC and AT also played a significant role as drivers. The area was a net annual source for atmospheric $CO_2$ of size 0.180±0.009 mol $CO_2$ $m^{-2}$ $y^{-1}$, with the spring to fall being the time for emission to the atmosphere, while the winter being the time for $CO_2$ absorption by the sea surface.

We augmented the mooring data with data from literature all together covering the period 1977 to 2015 and assessed the long-term trends in $pCO_2^w$, which were determined for the seasons winter–spring and summer-fall of size 1.75 ± 0.72 $\mu$atm $y^{-1}$ and 1.80 ± 0.41 $\mu$atm $y^{-1}$, respectively. These are weaker trends compared to that of the atmosphere (1.96 ± 0.02 $\mu$atm $y^{-1}$), and we speculate that the area has transformed from being a source area for $CO_2$ to the atmosphere throughout the year to becoming a sink area for $CO_2$ during parts of the year. A similar transformation happened during the 2000s in the Mediterranean Sea. The long term $pCO_2^w$ trend was primarily driven by increasing DIC during all seasons, and during summer-fall seasons, increasing SST and TA also contributed significantly to the long-term $pCO_2^w$ trend. The increase in AT over the years was likely connected to the declining calcification rates in the central and southern Red Sea. However, the long term DIC and AT trends were highly uncertain due to the scarcity of data, highlighting the need for maintaining a long time series as presented in this study.

The new data presented in this manuscript represents the first semi-continuous $pCO_2^w$ dataset over a full annual cycle. Future elaboration of these data is expected to contribute to improved understanding of the annual cycle of pH and saturation concentration of calcite in this region.

## CRediT authorship contribution statement

**Elsheikh B. Ali:** Contributed with ideas, Most of the calculation, Most of the writing, Performing parts of the time series sampling and mooring deployment (Chief Scientist of the cruises). **Ingunn Skjelvan:** Contributed with ideas, Calculations, Writing. **Abdirahman M. Omar:** Contributed with ideas, Calculations, Writing. **Are Olsen:** Contributed with ideas, Discussion and comments. **Tor E. de Lange:** Contributed with deployment and retrieving of the mooring in addition to setup, Maintenance of the instruments used. **Truls Johannessen:** Contributed with ideas, Discussion, and comments. **Salma Elageed:** Contributed with calculations.

## Declaration of competing interest

The authors declare that they have no known competing financial interests or personal relationships that could have appeared to influence the work reported in this paper.

## Acknowledgements

This work was part of a PhD project at the University of Bergen, Norway, funded by the Norwegian Quota program. The work of I. Skjelvan and A.M. Omar was partly supported by the Research Council of Norway (RCN) through the project Michelsen Centre for Research-based Innovation in Measurements Science and Technology (MIMT). The mooring and attached instrumentation were funded by RCN through the projects MIMT and FME SUCCESS (Subsurface CO2 Storage – Critical Elements and Superior Strategy). We are grateful to the captain and crew of the Sudanese Sea Port Corporation tugboat used for deployment. We are thankful to Prof. Abdel Gadir D. El Hag and Prof. Mohamd E.A. Hamza (former directors of Institute of Marine Research; IMR) for their support and to the IMR staff for making this deployment possible.

## Appendix A. Supplementary data

Supplementary material related to this article can be found online at https://doi.org/10.1016/j.rsma.2021.101796.

## References

Alawad, K.A., Al-Subhi, A.M., Alsaafani, M.A., Alraddadi, T.M., 2020. Decadal variability and recent summer warming amplification of the sea surface temperature in the red sea. PLoS One 15 (9), e0237436, https://doi.org/10.1371/journal.pone.0237436.

Ali, E.B., 2008. The Inorganic Carbon Cycle in the Red Sea (Master's thesis). Geophysical Institute, University of Bergen, Bergen, Norway, p. 77.

Ali, E.B., 2017. The Inorganic Carbon Cycle of the Red Sea (Ph.D. thesis). University of Bergen, https://bora.uib.no/bora-xmlui/h{and}le/1956/16944.

Ali, E.B., Churchill, J.H., Barthel, K., Skjelvan, I., Omar, A.M., de Lange, T.E., Eltaib, E.B.A., 2018. Seasonal variations of hydrographic parameters off the Sudanese coast of the Red Sea, 2009-2015. Reg. Stud. Mar. Sci. J. 18.

Beauverger, C., 1984a. MD 33/MEROU a bord du "MARION DUFRESNE" ]6 juin au 4 juillet 1982, 25 septembre au 4 octobre 1982. Les rapports des campagnes a la mer, publication des T.A.A.F. No. 82-05. p. 163.

Beauverger, C., Brunet, C., Poisson, A., 1984b. MD 33/MEROU a bord du "MARION DUFRESNE" 16 juin au 4 juillet 1982, 25 septcmbre au 4 octobre 1982. Les rapports des campagnes ala mcr, publication des T.A.A.F. No. 82-04. p. 181.

Behrenfeld, M.J., O'Malley, R., Siegel, D., McClain, C., Sarmiento, J., Feldman, G., Milligan, A., Falkowski, P., Letelier, R., Boss, E., 2006. Climate-driven trends in contemporary ocean productivity. Nature 444, 752–755.

Chaidez, V., Dreano, D., Agusti, S., Duarte, C.M., Hoteit, I., 2017. Decadal trends in Red Sea maximum surface temperature. Sci. Rep. 7, 8144. http://dx.doi.org/10.1038/s41598-017-08146-z.

CMEMS, 2019. Global ocean surface carbon product multi-obs_Glo_Bio_Carbon_Surface_Rep_015_008, e.u. Copernicus marine service information.

Dai, M., Cao, Z., Guo, X., Zhai, W., Liu, Z., Yin, Y., Gan, J., Hu, 2013. Why are some marginal seas sources of atmospheric CO2? Geophys. Res. Lett. 40, 2154–2158. http://dx.doi.org/10.1002/grl.50390.

Denvil-Sommer, A., Gehlen, M., Vrac, M., Mejia, C., 2019. LSCE-FFNN-v1: a two-step neural network model for the reconstruction of surface ocean pCO2 over the global ocean. Geosci. Model Dev. 12, 2091–2105, https://doi.org/10.5194/gmd-12-2091-2019.

Dickson, A.G., 1990. Standard potential of the reaction: AgCl(s) + 1/2 $H_2$(g) = Ag(s) + HCl(aq), and the standard acidity constant of the ion $HSO_4^-$ in synthetic sea water from 273.15 to 318.15 K. J. Chem. Thermodyn. 22, 113–127.

Dickson, A.G., Millero, F.J., 1987. A comparison of the equilibrium constants for the dissociation of carbonic acid in seawater media. Deep-Sea Res. 34, 1733–1743.

Dickson, A.G., Sabine, C.L., Christian, J.R., 2007. Guide To Best Practices for Ocean $CO_2$ Measurements, vol. 3. PICES Special Publication, p. 191.

Dlugokencky, E., Tans, P., 2020. Trends in Atmospheric Carbon Dioxide. National Oceanic & Atmospheric Administration, Earth System Research Laboratory (NOAA/ESRL), Available at: http://www.esrl.noaa.gov/gmd/ccgg/trends/global.html.

FAO, 1989. The state of food and agriculture. FAO Agriculture Series 22 (188).

Friedlingstein, P., Jones, M.W., O'Sullivan, M., Andrew, R.M., Hauck, J., Peters, G.P., Peters, W., Pongratz, J., Sitch, S., Quéré, C.Le., Bakker, D.C.E., Canadell, J.G., Ciais, P., Jackson, R.B., Anthoni, P., Barbero, L., Bastos, A., Bastrikov, V., Becker, M., Bopp, L., Buitenhuis, E., Chandra, N., Chevallier, F., Chini, L.P., Currie, K.I., Feely, R.A., Gehlen, M., Gilfillan, D., Gkritzalis, T., Goll, D.S., Gruber, N., Gutekunst, S., Harris, I., Haverd, V., Houghton, R.A., Hurtt, G., Ilyina, T., Jain, A.K., Joetzjer, E., Kaplan, J.O., Kato, E., Goldewijk, K.Klein., Korsbakken, J.I., Landschützer, P., Lauvset, S.K., Lefèvre, N., Lenton, A., Lienert, S., Lombardozzi, D., Marland, G., McGuire, P.C., Melton, J.R., Metzl, N., Munro, D.R., Nabel, J.E.M.S., Nakaoka, S.-I., Neill, C., Omar, A.M., Ono, T., Peregon, A., Pierrot, D., Poulter, B., Rehder, G., Resplandy, L., Robertson, E., Rödenbeck, C., Séférian, R., Schwinger, J., Smith, N., Tans, P.P., Tian, H., Tilbrook, B., Tubiello, F.N., van der Werf, G.R., Wiltshire, A.J., Zaehle, S., 2019. Global carbon budget 2019. Earth Syst. Sci. Data 11, 1783–1838. http://dx.doi.org/10.5194/essd-11-1783-2019.

Hydes, D., Jiang, Z.-P., Hartman, M.C., Campbell, J., Hartman, S.E., Pagnani, B.A., 2011. Dissolved inorganic carbon, alkalinity, temperature, salinity and DISSOLVED OXYGEN collected from profile and discrete sample observations using Alkalinity titrator, CTD and other instruments from the Pacific Celebes in the Alboran Sea, Arabian Sea and others from 2007-06-11 to 2012-03-18 (NCEI Accession 0081040). [Here used DIC, AT, T, S]. Dataset. https://doi.org/10.3334/cdiac/otg.vos_pc_2007-2012. (Accessed 22 February 2021).

Johnson, K.M., Wills, K.D., Butler, D.B., Johnson, W.K., Wong, C.S., 1993. Coulometric total carbon dioxide analysis for marine studies. Mar. Chem. 44, 167–187.

Kalnay, E., et al., 1996. The NCEP/NCAR 40-year reanalysis project. Bull. Am. Meteorol. Soc. 77, 437–471.

Key, R.M., Olsen, A., van Heuven, S., Lauvset, S.K., Velo, A., Lin, X., Schirnick, C., Kozyr, A., Tanhua, T., Hoppema, M., Jutterström, S., Steinfeldt, R., Jeansson, E., Ishii, M., Pérez, F.F., Suzuki, T., 2015. Global Ocean Data Analysis Project, Version 2 (GLODAPv2), ORNL/CDIAC-162, NDP-P093. Carbon Dioxide Information Analysis Center, Oak Ridge National Laboratory, US Department of Energy, Oak Ridge, Tennessee, http://dx.doi.org/10.3334/CDIAC/OTG.NDP093_GLODAPv2.

Klaus, R., 2015. Coral reefs and communities of the central and southern Red Sea (Sudan, Eritrea, Djibouti, and Yemen). In: Rasul, Stewart (Eds.), The Red Sea. Springer Earth System Sciences, ISBN: 978-3-662-45201-1, p. 638.

Körtzinger, A., 1999. Determination of carbon dioxide partial pressure ($pCO_2$). In: Grasshoff, K., Kremling, K., Ehrhardt, M. (Eds.), Methods of Seawater Analysis. Wiley-VCH, pp. 149–158.

Landschützer, P., Laruelle, G.G., Roobaert, A., Regnier, P., 2020. A uniform pCO2 climatology combining open and coastal oceans. Earth Syst. Sci. Data 12, 2537–2553, https://doi.org/10.5194/essd-12-2537-2020.

Laruelle, G.G., Landschützer, P., Gruber, N., Tison, J.-L., Delille, B., Regnier, P., 2017. Global high-resolution monthly $pCO_2$ climatology for the coastal ocean derived from neural network interpolation. Biogeosciences 14, 4545–4561, https://doi.org/10.5194/bg-14-4545-2017.

Liss, P.S., Merlivat, L., 1986. Air-sea gas exchange rates: introduction and synthesis. In: Buat-Menard, P. (Ed.), The Role of Air-Sea Exchange in Geochemical Cycling. In: NATO ASI Series C: Mathematical and Physical Sciences, vol. 185, D. Reidel Publishing Company, pp. 113–127.

Mehrbach, C., Culberson, C.H., Hawley, J.E., Pytkowicz, R.M., 1973. Measurement of the apparent dissociation constants of carbonic acid in seawater at atmospheric pressure. Limnol. Oceanogr. 18, 897–907.

Metzl, N., 2016. Partial pressure (or fugacity) of carbon dioxide, salinity and other variables collected from surface underway observations using barometric pressure sensor, carbon dioxide ($CO_2$) gas analyzer and other instruments from MARION DUFRESNE in the Arabian Sea, Gulf of Aden and others from 1999-10-18 to 1999-11-01 (NCEI Accession 0157283). Dataset. NOAA National Centers for Environmental Information, https://doi.org/10.3334/cdiac/otg.minerve_40_1999.

Metzl, N., Moore III, B., Papaud, A., Poisson, A., 1989. Transport and carbon exchange in Red Sea inverse methodology. Glob. Biogeochem. Cycle 3 (1), 1–26.

Metzl, N., Poisson, A., Louanchi, F., Brunet, C., Schauer, B., Bres, B., 1995. Spatio-temporal distributions of air-sea fluxes of $CO_2$ in the Indian and Antarctic Oceans: a first step. Tellus 47B, 56–69.

Nightingale, P.D., Malin, G., Law, C.S., Watson, A.J., Liss, P.S., Liddicoat, M.I., Boutin, J.R.C., Upstill-Goddard, R.C., 2000. In-situ evaluation of air-sea gas exchange parameterizations using novel conservative and volatile tracers. Glob. Biogeochem. Cycles 14, 373–387.

Olsen, A., Key, R.M., van Heuven, S., Lauvset, S.K., Velo, A., Lin, X., Schirnick, C., Kozyr, A., Tanhua, T., Hoppema, M., Jutterström, S., Steinfeldt, R., Jeansson, E., Ishii, M., Pérez, F.F., Suzuki, T., 2016. The global ocean data analysis project version 2 (GLODAPv2) – an internally consistent data product for the world ocean. Earth Syst. Sci. Data 8, 297–323.

Raitsos, D.E., Lavender, S.J., Maravelias, C.D., Haralabous, J., McQuatters-Gollop, A., Edwards, P.C., 2011. Macroscale factors affecting diatom abundance: A synergistic use of continuous plankton recorder and satellite remote sensing data. Int. J. Remote Sens. 32, 2081–2094. http://dx.doi.org/10.1080/01431161003645832.

Rasul, N.M.A., Stewart, I.C.F., Nawab, Z.A., 2015. Introduction to the Red Sea: Its origin, structure, and environment. In: Rasul, Stewart (Eds.), The Red Sea. Springer Earth System Sciences, ISBN: 978-3-662-45201-1, p. 638.

Rhein, M., Rintoul, S.R., Aoki, S., Campos, E., Chambers, D., Feely, R.A., Gulev, S., Johnson, G.C., Josey, S.A., Kostianoy, A., Mauritzen, C., Roemmich, D., Talley, L.D., Wang, F., 2013. Observations: Ocean. In: Stocker, T.F., Qin, D., Plattner, G.-K., Tignor, M., Allen, S.K., Boschung, J., Nauels, A., Xia, Y., Bex, V., Midgley, P.M. (Eds.), Climate Change 2013: The Physical Science Basis. Contribution of Working Group I To the Fifth Assessment Report of the Intergovernmental Panel on Climate Change. Cambridge University Press, Cambridge, United Kingdom and New York, NY, USA.

Schlitzer, R., 2020. Ocean data view. odv.awi.de.

Sofianos, S.S., Johns, W.E., 2002. An oceanic general circulation model (OGCM) investigation of the Red Sea circulation, 1. Exchange between the Red Sea and the Indian Ocean. J. Geophys. Res. 107, 3196. http://dx.doi.org/10.1029/2001JC001184.

Souvermezoglou, T., Metzl, N., Poisson, A., 1989. Red Sea budgets of salinity, nutrients and carbon calculated in the Strait of Bab Al Mandab during summer and winter seasons. J. Mar. Res. 47, 441–456.

Steiner, Z., Turchyn, A.V., Harpaz, E., Silverman, J., 2018. Water chemistry reveals a significant decline in coral calcification rates in the southern Red Sea. Nature comms. http://dx.doi.org/10.1038/s41467-018-06030-6.

Sweeney, C., Gloor, E., Jacobson, A.R., Key, R.M., McKinley, G., Sarmiento, J.L., Wanninkhof, R., 2007. Constraining global air-sea gas exchange for CO2 with recent bomb C-14 measurements. Glob. Biogeochem. Cycle 21, GB2015. http://dx.doi.org/10.1029/2006gb002784.

Taillandier, V., D'Ortenzio, F., Antoine, D., 2012. Carbon fluxes in the mixed layer of the Mediterranean Sea in the 1980s and the 2000s. Deep Sea Res. I 65, 73–84.

Takahashi, T., Olafsson, J., Goddard, J., Chipman, D.W., Sutherland, S.C., 1993. Seasonal variation of $CO_2$ and nutrients in the high-latitude surface oceans: A comparative study. Glob. Biogeochem. Cycles 7, 843–878.

Takahashi, T., Sutherland, S.C., Sweeney, C., Poisson, A., Metzl, N., Tilbrook, B., Bates, N., Wanninkhof, R., Feely, R.A., Sabine, C., Olafsson, J., Nojiri, Y., 2002. Global sea–air CO2 flux based on climatological surface ocean $pCO_2$, and seasonal biological and temperature effects. Deep Sea Res. II 49 (9–10), 1601–1622.

Tragou, E., Garrett, C., Outerbridge, R., Gilman, C., 1999. The heat and freshwater budgets of the Red Sea. J. Phys. Oceanogr. 29, 2504–2522.

Uppström, L.R., 1974. Boron/chlorinity ratio of deep-sea water from the Pacific Ocean. Deep Sea Res. 21, 161–162.

van Heuven, S., Pierrot, D., Rae, J.W.B., Lewis, E., Wallace, D.W.R., 2011. MATLAB Program Developed for CO2 System Calculations. ORNL/CDIAC-105b. Carbon Dioxide Information Analysis Center, Oak Ridge National Laboratory, U.S. Department of Energy, Oak Ridge, Tennessee, http://dx.doi.org/10.3334/CDIAC/otg.CO2SYS_MATLAB_v1.1.

Wanninkhof, R., 1992. Relationship between wind speed and gas exchange over the ocean. J. Geophys. Res. 97 (C5), 7373–7382.

Wanninkhof, R., 2014. Relationship between wind speed and gas exchange over the ocean revisited. Limnol. Oceanogr. Meth. 12 (2014), 351–362.

Weiss, R.F., 1974. Carbon dioxide in water and seawater: the solubility of a non-ideal gas. Mar. Chem. 2, 203–215.

Weiss, R.F., Broecker, W.S., Craig, H.B., Spencer, D.W., 1983. Geosecs Indian Ocean Expedition, vol. 5. In: Hyd. Data. Nat. Sc. Fond., U.S. Government Print. Off.

Zolina, O., Dufour, A., Gulev, S.K., Stenchikov, G., 2017. Regional hydrological cycle over the Red Sea in ERA-Interim. J. Hydrometeorol. 18, 65–83.